Dynamics and rheology of highly deflated vesicles

ESAIM: PROCEEDINGS, August 2009, Vol. 28, p. 211-226
M. Ismail, B. Maury & J.-F. Gerbeau, Editors

DYNAMICS AND RHEOLOGY OF HIGHLY DEFLATED VESICLES

Giovanni Ghigliotti[1], Hassib Selmi[2], Badr Kaoui[1], George Biros[3] and Chaouqi Misbah[1]

Abstract. We study the dynamics and rheology of a single two-dimensional vesicle embedded in a linear shear flow by means of numerical simulations based on the boundary integral method.
The viscosities inside and outside the vesicle are supposed to be identical. We explore the rheology by varying the reduced area, i.e. we consider more and more deflated vesicles. Effective viscosity and normal stress differences are computed and discussed in detail, together with the inclination angle and the lateral membrane velocity (tank-treading velocity). The angle is found, surprisingly, to reach a zero value (flow alignment) at a critical reduced area even in the absence of viscosity contrast.
A Fast Multipole Method is presented that enables to run efficiently simulations with a large number of vesicles. This method prevails over the direct summation for a number of mesh points beyond a value of about 10^3. This offers an interesting perspective for simulation of semi-dilute and concentrated suspensions.

Résumé. On étudie la dynamique et la rhéologie d'une vésicule bidimensionnelle immergée dans un écoulement de cisaillement linéaire en utilisant la méthode des intégrales de frontière.
La viscosité à l'intérieur de la vésicule est prise identique à celle du liquide porteur et nous faisons varier la surface réduite, c.-à-d. nous considérons des vésicules de plus en plus dégonflées. La viscosité effective et la différence des contraintes normales sont calculées et discutées en détail, ainsi que l'angle d'inclinaison de la vésicule et la vitesse latérale (de type chenille de char) de la membrane. De façon surprenante on trouve que l'angle d'inclinaison atteint zéro même en l'absence de contraste de viscosité, et ce pour une valeur critique de l'aire réduite.
Une Méthode de Multipoles Rapides est présentée comme un outil permettant de réaliser des simulations avec un grand nombre de vésicules. Cette méthode est plus rapide que la sommation directe pourvu que le nombre de points considéré est au delà d'une valeur de l'ordre de 10^3. Ce résultat offre des perspectives intéressantes en vue de simulations de suspensions semi-diluées et concentrées.

Introduction

Understanding microscopic blood dynamics and its impact on macroscopic flow properties, i.e. rheology, continues to present a significant challenge [1,2]. This is so because of an intimate coupling between the complex dynamical microscopic structure, represented by deformable cells (mainly red blood cells, that constitute the major component of blood) and the suspending Newtonian fluid, the plasma. This is a micro/macro coupling problem par excellence. Due to this coupling blood rheology acquires a non Newtonian nature. Blood is

[1] Laboratoire de Spectrométrie Physique, CNRS - Université Joseph Fourier / UMR 5588, BP 87, 38402 Saint Martin d'Hères, France. e-mail: gghiglio@spectro.ujf-grenoble.fr
[2] Laboratoire d'Ingénierie Mathématique, Ecole Polytechnique de Tunisie B.P. 743 - 2078 La Marsa, Tunisia
[3] Georgia Institute of Technology, 1324 Klaus Advanced Computing Building, 266 Ferst Drive, Atlanta GA 30332-0765

Article published by EDP Sciences and available at http://www.edpsciences.org/proc or http://dx.doi.org/10.1051/proc/2009048

also referred to as a *viscoelastic* fluid, or a complex fluid. The viscous behavior arises from the fluids in presence (plasma and hemoglobin), while elastic properties stem from shear and bending elasticity of the red cell membrane. In order to gain insight towards this multiscale problem, it is highly desirable to elucidate first the basic elementary processes by focusing on simplified systems that lend themselves to a relatively easy modeling, while keeping the basic physical ingredients. A suspension of phospholipidic vesicles constitutes a potential model candidate, since it circumvents the still debated problem of mechanics of the cytoskeleton raised by the red blood cells. Further progress should later then be achieved by a progressive refinement of concepts.

A vesicle is a simple model to describe a red blood cell (RBC): it is made of a closed membrane composed of a phospholipidic double layer (the main ingredient of the cellular membrane) encapsulating a Newtonian fluid. The bi-layer is fluid at room as well as at physiological temperature, and can thus be viewed as a two dimensional incompressible fluid. Since RBCs are simple eucaryotic cells (i.e. they are devoid of a nucleus), they differ (from the mechanical point of view) from vesicles mainly by the presence of an elastic cytoskeleton (that is believed to maintain RBCs integrity under high enough shear rates). Despite this difference, vesicles are considered as an adequate description to understand the basic mechanisms governing the dynamics of RBCs, thanks to the central role played by the membrane [3, 4]. We shall thus focus on this model system in order to infer and identify some key points playing a role in rheology of RBC suspensions, while leaving progressive refinement to the future.

We consider a two-dimensional vesicle suspended in a Newtonian fluid and submitted to a linear shear flow. Moreover, the viscosity contrast (i.e. the ratio between the viscosity of the internal fluid over the viscosity of the suspending one) is set to unity.

We neglect hydrodynamic interactions among vesicles, in that we consider a dilute enough suspension. We first consider a single vesicle by studying its dynamics and then discuss how rheological properties can be extracted in the dilute regime (low enough volume fraction so that disregarding hydrodynamic interactions makes sense [5, 6]).

Studies on vesicle rheology have been considered analytically only recently in the small deformation regime [7, 8] (a quasi-spherical shape), an extension to shapes which deviate significantly from a sphere can be handled only numerically. This regime is challenging because large deviations from a sphere set severe numerical limitations on precision, time steps, etc... due to the fact that the membrane force (curvature force) involves fourth order derivatives. In addition, one has to fulfill local membrane incompressibility (recall that the membrane is a two dimensional incompressible fluid).

Restricting to two-dimensional simulations allows one to significantly lower the computational time. Since many phenomena found in two dimensions (e.g. bifurcation from tank-teading to tumbling [9]) are observed in three dimensions experimentally, this gives confidence that focusing on two dimensions may already capture the essential features. This paper combines a numerical and mathematical study with physical concepts to extract new features not explored so far. Of particular interest is the discovery that the inclination angle of a vesicle in a shear flow can attain zero (flow alignment) even in the absence of a viscosity contrast, provided that the vesicle is deflated enough. This will have an impact on rheology.

Several numerical methods for vesicle dynamics have been used so far. Without being exhaustive, the main methods are: boundary integral method (BIM) [4, 10–12], multiparticle collision dynamics [13], phase field [14] and level-set methods [15]. To date it seems that BIM produces the most precise results. Moreover, while the other methods solve the dynamics in the whole bulk fluid, BIM offers a numerical advantage of solving a N-dimensional problem by computing $(\mathrm{N}-1)$-dimensional integrals: only the boundaries of the fluid domains need to be discretized. This is done at a certain price: nonlocality, which imposes that the method is $O(N^2)$ (N being the number of mesh points on the vesicle). However, use of a fast multipole expansion will be able to achieve a $O(N)$ algorithm.

In this paper we adopt the BIM. In our simple model where no external boundary is present, only the vesicle membrane has to be discretized and evolved in time, making the solution extremely efficient in term of computing time.

The challenges still present in this model are intrinsic to the physics of the problem, and related to the nature

of the forces exherted by the membrane on the surrounding fluid: their computation requires high precision on the discretisation of the differential operators on the curved surface of the vesicle.

1. The physical model

We consider a two-dimensional vesicle embedded in a Newtonian fluid. The vesicle is a closed liquid membrane, locally incompressible and endowed with a bending energy. The internal area (in two dimensions) of the vesicle is conserved due to the incompressibility assumed for the internal fluid. The velocity field is considered to be continuous across the membrane, since we assume no-slip condtions on the membrane [3, 4, 11, 16].
We consider the Stokes limit (we neglect inertia, i.e. we consider the zero Reynolds number limit), which is consistent with available experimental data on vesicles [17, 18].
We list below the starting model equations.
The fluid is assumed to obey Stokes equation, then the momentum conservation condition reads

$$\nabla p - \eta \nabla^2 \mathbf{u} + \mathbf{f} = 0 \tag{1}$$

where $\mathbf{u}$ is the velocity, p is the pressure and η is the viscosity of the fluid, and the incompressibility condition is expressed as

$$\nabla \cdot \mathbf{u} = 0 \tag{2}$$

$\mathbf{f}$ is the force exerted by the membrane on the fluid. This force is composed of two contributions, the first one arising from the bending energy of the membrane, and the second one from the energy associated with the constraint of local incomprssibility of the membrane. The bending energy of the membrane is

$$E_B = \kappa_B \int_\gamma \frac{[c(s)]^2}{2} ds \tag{3}$$

where γ represents the membrane contour, s the curvilinear coorinate along it, $c(s)$ is the local curvature of the contour and κ_B is the bending modulus.
The incompressibility constraint imposed on the vesicle membrane is written as:

$$\nabla_\gamma \cdot \mathbf{u} = 0 \tag{4}$$

where ∇_γ is the gradient operator along the contour of the vesicle and $\mathbf{u}$ the velocity field of the adjacent fluid. This constraint can be expressed by the use of a local Lagrangian multiplier $\zeta(s)$, giving the energy the form

$$E_\zeta = \int_\gamma \zeta(s) ds \tag{5}$$

The variation of the total energy E_T, defined as the sum of the two contributions $E_T = E_B + E_\zeta$, gives then the expression of the force:

$$\mathbf{f}(\mathbf{x}) \equiv -\frac{\delta E_T}{\delta \mathbf{x}} = -\kappa_B \left[\frac{d^2 c}{ds^2} + \frac{1}{2} c^3 \right] \mathbf{n} + \zeta c \mathbf{n} + \frac{d\zeta}{ds} \mathbf{t} \tag{6}$$

where $\mathbf{n}$ and $\mathbf{t}$ are the outward normal and tangent vector to the contour (for a complete derivation of the force, see [19]).

From this formulation we can see how the bending force is always along the normal direction, as for the bending of an elastic ladder. Interestingly, the tension-like contribution has components not only in the tangential direction (as it would look natural to guarantee the incompressibility of the contour), but also in the normal one. This can be understood by thinking that these tension-like forces are tangential to a curved contour, and thus their sum can have a component out of the tangential line: infact the normal contribution is proportional to the local curvature c.

2. The boundary integral method

Owing to the linearity of the Stokes equation use can be made of the boundary integral formulation [4, 10, 16, 20, 21] which allows one to express the perturbation of the vesicle on the velocity of the fluid in terms of an integral of the force (times a Green's kernel) computed on the membrane of the vesicle, which represents the only boundary in the present study (we consider an unbounded shear flow):

$$\mathbf{u}(\mathbf{x}_0) = \mathbf{u}^\infty(\mathbf{x}_0) + \frac{1}{4\pi\eta}\int_\gamma G(\mathbf{x}-\mathbf{x}_0)\cdot\mathbf{f}(\mathbf{x})d\mathbf{x} \tag{7}$$

where

$$G_{ij}(\mathbf{x}-\mathbf{x}_0) = -\delta_{ij}\ln|\mathbf{x}-\mathbf{x}_0| + \frac{(\mathbf{x}-\mathbf{x}_0)_i(\mathbf{x}-\mathbf{x}_0)_j}{|\mathbf{x}-\mathbf{x}_0|^2} \tag{8}$$

is the Green function of the two-dimensional problem [20]. $\mathbf{x}$ is the source point represented by the Green's function itself. $\mathbf{u}^\infty(\mathbf{x}_0)$ represents the imposed flow (in our case, the linear shear) computed at point $\mathbf{x}_0$. This is a free-boundary problem, in that the vesicle shape is not known a priori. Thus despite the fact that the bulk Stokes equation is linear, the shape evolution equation is both nonlinear and nonlocal.

The above equation has been solved numerically by several authors [4, 11, 16]. We adopt for this study the code written by Veerapaneni *et al.* [12], that includes a high-precision algorithm for the computation of geometrical quantities, allowing to explore significantly deflated vesicles, as show in the following.

We do not get into the details of the implementation of the numerical code (which can be found in [12]), here we shall merely focus on the main physical results and their far reaching consequences. Despite that, we shall describe here the general ideas.

Starting from the position of the boundary, the integral equation provides us with the velocity of the boundary itself. Once the velocity is obtained, its value is used to update the position of the boundary itself using a first-order semi-implicit scheme. The iteration of this procedure allows the computation of the time evolution.
The position of the membrane is decomposed on a Fourier basis (via an intermidiate passage through a regular parametrization of the interface). The switch between $\mathbf{x}$ and its Fourier transform $\hat{\mathbf{x}}$ is done using FFT. The use of Fourier transform allows to gain spectral precision in the computation of surface derivatives, which represent the main challenge for a numerical solution of vesicle dynamics, due to the form of the membrane force (6) containing fourth-order derivatives (in the form of a second derivative of the curvature, being itslef a second derivative of the position of the membrane). Previous studies [4, 11, 16] used a standard finite difference technique, leading to some loss of precision in the computation of high-order derivatives.

3. Tank-treading regime for $C_a = 1$

In this section we analyze the tank-treading regime of a vesicle having the same viscosity η of the embedding fluid. The imposed flow is taken as $\mathbf{u}^\infty(\mathbf{x}_0) = \dot\gamma y\mathbf{e}_x$, where $\dot\gamma$ denotes the shear rate. The flow strength is determined by a dimensionless number, which may be named a capillary number (in analogy with drops)

$$C_a = \frac{\eta\dot\gamma r_0^3}{\kappa_B} \tag{9}$$

which compares the time scale of the imposed shear ($\dot\gamma^{-1}$) to the time scale of the relaxation of the vesicle due to bending forces ($\eta r_0^3/\kappa_B$). r_0 is the radius of the circle having the same perimeter as the actual vesicle. For definiteness we set $C_a = 1$ for all the simulations presented in this paper. This value is intermediate between the regime dominated by membrane bending energy ($C_a \ll 1$) and the one dominated by the imposed shear ($C_a \gg 1$). Thus for $C_a = 1$ the physics will depend on both ingredients, as discussed in more detail below.
The dimensionless parameter of interest in the present study is the reduced area enclosed by the vesicle, α,

which is defined by

$$\alpha = \frac{[A/\pi]}{[L/2\pi]^2} \tag{10}$$

where A is the enclosed area and L is the vesicle perimeter. For a circle $\alpha = 1$, otherwise α is always smaller than unity. The more deflated the vesicle is, the smaller is the reduced area. We have scanned values of α in the interval $\alpha \in [0.32; 1.00]$ (see paragraph 3.1 and figure 1). These two limiting values are already numerically significant on their own for two different reasons:

- a circular vesicle ($\alpha = 1$) in a shear flow is a singular limit, since the round shape cannot balance the hydrodynamical constraints exerted on the surface, as pointed out in [4]. A singularity subtraction has been performed in order to be able to simulate precisely this situation [12];
- low values of the reduced area are difficult to reach because of the high curvature of the surface. It is the spectral precision in space (i.e. the use of Fourier transforms) that ensures precision and stability of the code in this region of the parameter space.

Moreover, the circular limit, although not very interesting by itself, is very important to check the accuracy of the results, since exact analytical solutions exist for the dynamics and rheology of non-interacting cylinders, as reported in detail in Appendix A [22–24].

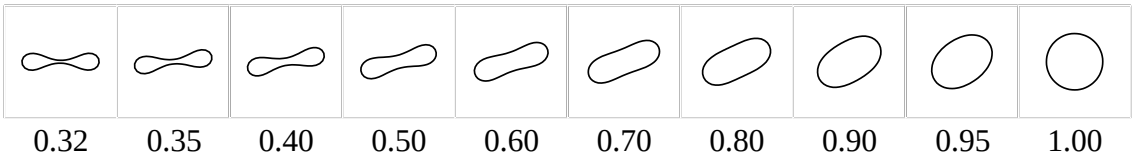

FIGURE 1. Stationary vesicle shapes with different reduced areas α under shear flow. The value of the reduced area α is reported below the corresponding shape.

3.1. **Dynamics: inclination angle, tank-treading velocity and bending energy**

To study the dynamics of the vesicle, we measure the inclination angle of the stationary shape, the velocity of the membrane and the bending energy associated with its shape.

In figure 2 we plot the inclination angle Ψ (measured from the direction of the imposed flow) of a tank-treading vesicle. The angle tends to $\Psi = 45°$ for a vesicle having a circular shape (see figure 1), as expected analytically [3], and numerically [4,11]. The surprising result is that the inclination angle goes to zero for a finite reduced area $\alpha_c = 0.32$. A viscosity contrast larger than one (meaning that the viscosity inside the vesicle is larger than that of the embedding fluid) is needed for larger α in order to achieve flow alignment. No stationary solution is stable below this limit, and then tank-treading cannot be observed below the critical value of the reduced area α_c. We expect tumbling to take place.

In figure 3 we plot the tank-treading velocity of the membrane, i.e. the membrane tangential velocity. Since the membrane is inextensible the magnitude of this velocity must be the same on all the points of the membrane. Its value decreases for a smaller reduced area of the vesicle. This is expected due to the fact that when α decreases the vesicle aligns further with the flow and the torque due to the imposed flow has been transferred more to inclination than to tank-treading. In the regime where the vesicle is circular we obtain for tank-treading velocity $v_{tt} = 0.502\ \dot{\gamma}$ in very good agreement with the exact analytical result $\dot{\gamma}/2$ (see Appendix A).

In figure 4 we plot the bending energy of the membrane (3): not surprisingly it increases with the deflation of the vesicle, since the curvature becomes locally higher.
We can compare the results with the value E_B^c for a circle of radius one (i.e. $c = 1$):

$$E_B^c = \int_0^{2\pi} \frac{c^2}{2} d\phi = \pi \tag{11}$$

and the numerical result obtained for a circular vesicle, $E_B^c = 3.138$.

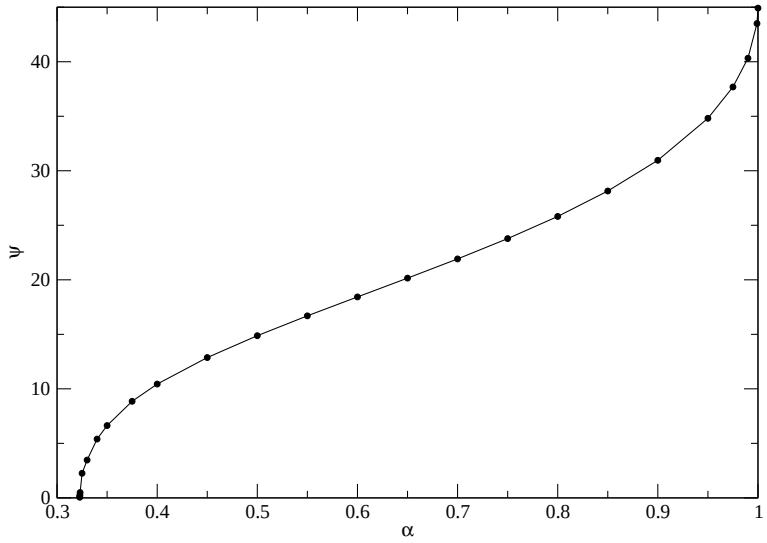

FIGURE 2. Inclination angle (in degrees) of a tank-treading vesicle in a shear flow for $C_a = 1$ as a function of the reduced area α.

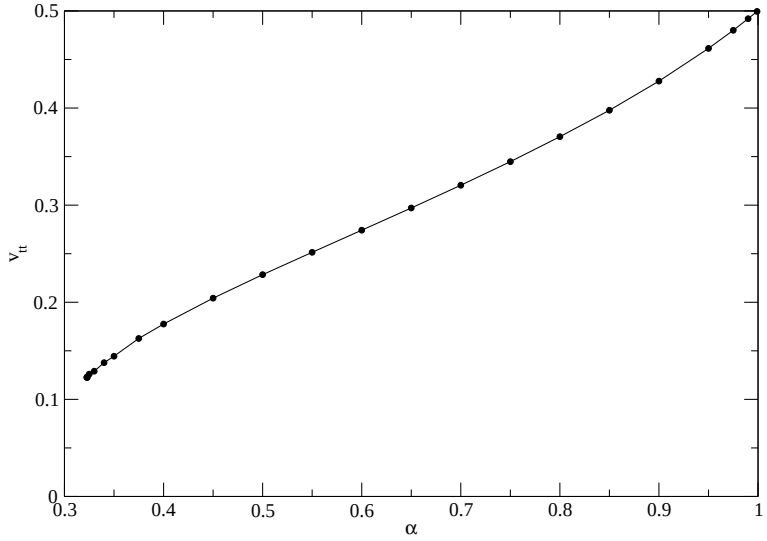

FIGURE 3. Tank-treading velocity measured in unit of $\dot{\gamma}$ as a function of the reduced area α.

3.2. **Rheology: effective viscosity and normal stress difference**

The rheological quantities that are investigated are the effective shear viscosity $\bar{\eta}_{eff}$ of the solution

$$\bar{\eta}_{eff} \equiv \frac{\langle \sigma_{xy} \rangle}{\dot{\gamma}} \tag{12}$$

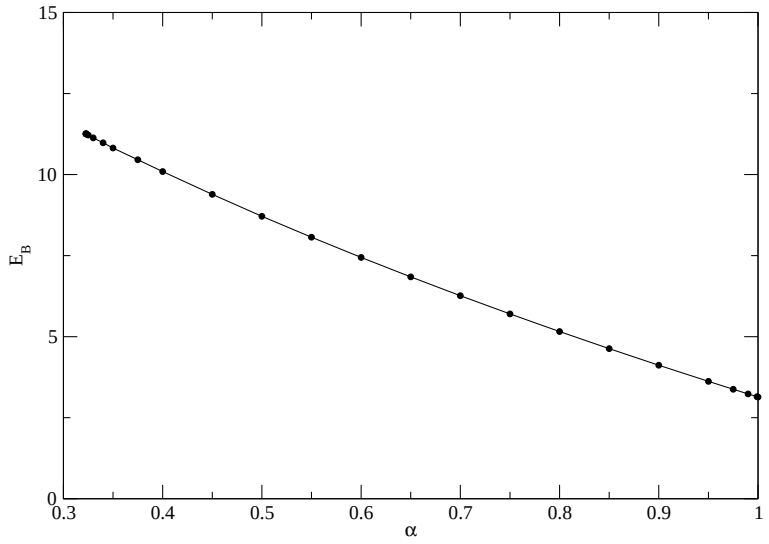

FIGURE 4. Curvature energy E_B of the membrane as a function of the reduces area α.

and the normal stress difference $\bar{N}$

$$\bar{N} \equiv \frac{\langle \sigma_{xx} \rangle - \langle \sigma_{yy} \rangle}{\dot{\gamma}} \tag{13}$$

where σ is the stress tensor of the suspension, $\dot{\gamma}$ the imposed shear rate and $\langle\ \rangle$ denotes volume (surface in two dimensions) average. It can be shown that the sample average over the whole fluid domain can be converted onto a contour integral.

In practice we normalize these quantities by subtracting the contribution of the imposed flow and dividing by the area fraction ϕ (in two dimensions) of the suspended entities. ϕ is defined as the ratio of the sum of vesicle areas over the total area. The imposed linear shear flow gives $\langle \sigma_{xy} \rangle = \eta\dot{\gamma}$ and $\bar{N} = 0$, so we have the dimensionless quantities:

$$\eta_{eff} \equiv \frac{\langle \sigma_{xy} \rangle - \eta\dot{\gamma}}{\eta\dot{\gamma}\phi} \tag{14}$$

and

$$N \equiv \frac{\langle \sigma_{xx} \rangle - \langle \sigma_{yy} \rangle}{\eta\dot{\gamma}\phi} \tag{15}$$

These are the same quantities computed analytically in [5, 6] for a suspension of rigid spheres and in [7, 8, 25] for vesicles.

In figure 5 we represent the effective viscosity, which is maximal for a circular vesicle and decreases for smaller reduced area. This can be explained as follows: the local incompressibility of the membrane ensures, in two dimensions, the uniformity of the velocity along the vesicle contour. So a deflated vesicle, having a smaller cross-section in the shear flow (see figure 1), imposes on it smaller constraints, resulting thus in a decrease of dissipation in the embedding fluid.

In the circular limit the effective viscosity coincides with the Einstein coefficient [5,6], representing the effective viscosity of a suspension of rigid spheres (or circles in the two-dimensional case). The Einstein coefficient is recovered within an error of 10^{-4}, that is we obtain $n_{eff} = 1.9999$ when the analytical result in two dimensions is $n_{eff} = 2$ [23, 24] (instead of 2.5 in three dimensions). Note that a circular vesicle, be it fluid inside or not, behaves exactly as a solid particle, since the enclosed fluid undergoes a global solid-like rotation enforced by the vesicle membrane.

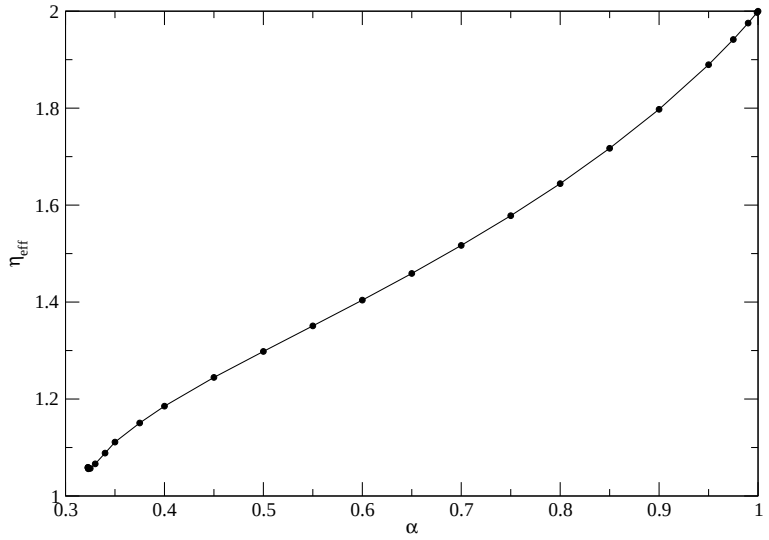

FIGURE 5. Effective viscosity η_{eff} of the dilute suspension of vesicles as a function of the reduces area α.

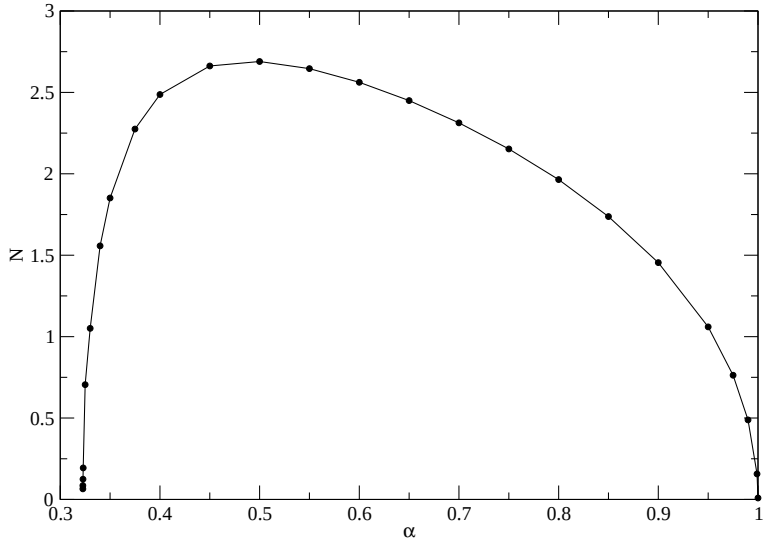

FIGURE 6. The normal stress difference N as a function of the reduced area α.

In figure 6 we plot the normal stress difference as a function of the reduced area. This rheological observable, normally linked to the elongation of elastic objects, is related here to the orientation of the vesicle in the flow. Its origin stems from the membrane force, since a pure Newtonian fluid (free of vesicles) cannot generate normal stress differences. In this situation the analytical solution is $N = 0$, while numerically we find $N = 0.0245$, providing the order of magnitude of numerical uncertainties on this quantity. We recover this value, $N \approx 0$ even at the opposite limit, $\alpha = \alpha_c$. Indeed at $\alpha = \alpha_c$ the vesicle is aligned with the flow, and this restores the up-down symmetry; actually we believe that normal stress difference is linked with the loss of this symmetry. Since we expect $N = 0$ for an up-down symmetric shape (at $\alpha = \alpha_c$ where the vesicle fully aligns with the flow,

and $\alpha = 1$ where the vesicle is circular), N must exhibit a maximum as shown in figure 6. The precise value of α at which the maximum should be expected is, at present, not yet completely understood.

4. Stability of the code and reliability of the results

The code used has been checked and compared to existing codes and showed high precision for the computation of dynamics and rheology of a single vesicle in the low-deformation regime. Far from the spherical limit the existing codes were not stable enough to be reliable, so we could not make comparison. Convergence tests have been done passing from 32 to 64 points on the membrane and from time steps of order 10^{-2} to 10^{-3}. The results are very satisfactory using the values $N = 64$ (discretization points) and $\Delta t = 10^{-3}$: the perimeter and area of the vesicles are very well preserved (errors usually less than 1‰ and less than 1% for the most deformed vesicles), the inclination angle converges rapidly and all the measured quantities look stable and noiseless. For completeness we will test the high deformation limit with a finer mesh and a shorter time step. Up to now, the simulations with these parameter values take too long to be run on a single CPU in reasonable time.

5. The Fast Multipole Method

Boundary Integral Method can easily be used to simulate a suspension of vesicles, where each entity is described via a mesh on its contour. Numerically this problem is $O(N^2)$, since for every point of the discretized system we have to compute the contributions coming from all the other points. It is then appealing to implement a fast algorithm to substitute the exact problem with an approximated one.
The objective of this study is to minimize the computing time of the matrix-vector product as well as the memory space reserved for the matrix storage by lowering the two costs from $O(N^2)$ to $O(N \log N)$ or even to $O(N)$.
In this context we introduce a scheme that allows for the resolution of Stokes problem in a 2D unbounded domain by coupling the fast multipole method (FMM), [26, 27] with the BIM.
The interest for using the FMM method lies in the reduction of the number of operations for the matrix-vector product, and the matrix storage, from $O(N^2)$ to $O(N)$. Such a method approximates the effect of distant points in the entire system as a set of points acting at long distance as a single multipole (multipole approximation and compression), while points in the direct proximity are handled exactly (i.e. a certain band of the matrix is stored in an exact way),
These schemes are made possible thanks to the variable separation of the Green function of the 2D Stokes operator, as shown below. This separation is the primary key of the development of the FMM method. More precisely, it allows the construction of multipole moments and transfer functions to obtain a $O(N \log N)$ scheme. Moreover we introduce other formulas of conversion and translation which are used to obtain a $O(N)$ scheme.

5.1. **Domain subdivision and tree representation**

At each time step, we start from a large imaginary square containing collocation points. This square represents the zeroth level of the tree (the top of the tree on the right panel of figure 7). We then make a recursive subdivision of the domain: the $n^{(th)}$ square is obtained by subdivision of the $n^{(th)} - 1$ square into 4 small squares (see figure 7), and so on. The level of the tree (i.e. the number of subdivision) is chosen after setting a desired accuracy ε. All collocation points are then distributed in several secondary areas. For each of them a multipolar moment is calculated and centered in the middle of the domain as well as the transfer function for the far field interaction in the corresponding domain.

Let us now apply this scheme to our problem. We have seen in section 1 and 2 that the velocity vector is given by equations (7) and (8).
The Green's function (8) can be written as follows:

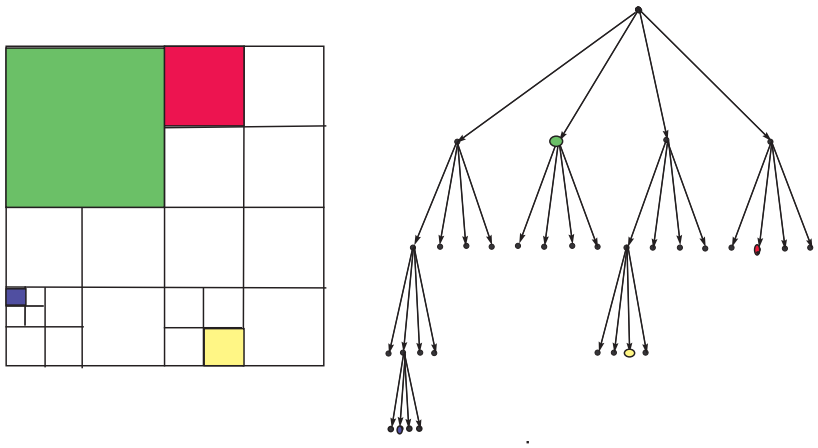

FIGURE 7. Tree representation (see text for explanation).

$$G(\mathbf{x}-\mathbf{x}_0) = G_l(\mathbf{x}-\mathbf{x}_0)\mathbf{1} + \frac{(\mathbf{x}-\mathbf{x}_0)\otimes(\mathbf{x}-\mathbf{x}_0)}{|\mathbf{x}-\mathbf{x}_0|^2} \tag{16}$$

where

$$G_l(\mathbf{x}-\mathbf{x}_0) = -\ln|\mathbf{x}-\mathbf{x}_0| \tag{17}$$

and

$$\frac{(\mathbf{x}-\mathbf{x}_0)\otimes(\mathbf{x}-\mathbf{x}_0)}{|\mathbf{x}-\mathbf{x}_0|^2}\mathbf{f}(\mathbf{x}) = -\nabla_x G_l(\mathbf{x}-\mathbf{x}_0) < \mathbf{f}(\mathbf{x})\cdot(\mathbf{x}-\mathbf{x}_0) > \tag{18}$$

where $< ... >$ denotes the ordinary scalar product. To evaluate equation (7), we have to use the form (16) of the Green's function, and equality (18), so that

$$\begin{aligned}
\mathbf{u}(\mathbf{x}_0) &= \frac{1}{4\pi\eta}\left[\int_\gamma G_l(\mathbf{x}-\mathbf{x}_0)\mathbf{1}\cdot\mathbf{f}(\mathbf{x})d\mathbf{x} + \int_\gamma \frac{(\mathbf{x}-\mathbf{x}_0)\otimes(\mathbf{x}-\mathbf{x}_0)}{|\mathbf{x}-\mathbf{x}_0|^2}\cdot\mathbf{f}(\mathbf{x})d\mathbf{x}\right] \\
&= \frac{1}{4\pi\eta}\left[\int_\gamma G_l(\mathbf{x}-\mathbf{x}_0)\mathbf{1}\cdot\mathbf{f}(\mathbf{x})d\mathbf{x} + \int_\gamma \nabla_x G_l(\mathbf{x}-\mathbf{x}_0)(< \mathbf{f}(\mathbf{x})\cdot\mathbf{x}_0 > - < \mathbf{f}(\mathbf{x})\cdot\mathbf{x} >)d\mathbf{x}\right] \\
&= \frac{1}{4\pi\eta}\left[\int_\gamma G_l(\mathbf{x}-\mathbf{x}_0)\mathbf{1}\cdot\mathbf{f}(\mathbf{x})d\mathbf{x} + (\mathbf{x}_0)_1\nabla_x\int_\gamma G_l(\mathbf{x}-\mathbf{x}_0)f_1(\mathbf{x})d\mathbf{x} + (\mathbf{x}_0)_2\nabla_x\int_\gamma G_l(\mathbf{x}-\mathbf{x}_0)f_2(\mathbf{x})d\mathbf{x}\right. \\
&\quad \left. -\nabla_x\int_\gamma G_l(\mathbf{x}-\mathbf{x}_0) < \mathbf{f}(\mathbf{x})\cdot\mathbf{x} > d\mathbf{x}\right]
\end{aligned}$$

The essential aim is to calculate rapidly and efficiently a typical quantity which enters above, which can be written as:

$$\int_\gamma G_l(\mathbf{x}-\mathbf{x}_0)q(\mathbf{x})d\mathbf{x} \tag{19}$$

where q is a scalar field that is equal to f_1, f_2 (the force components along the two cartesian axes) or $< \mathbf{f}\cdot\mathbf{x} >$. In what follows we are interested in the evaluation of the finite sum obtained after discretization of (19)

$$\Psi(\mathbf{x}_0) = \sum_{i=1}^{N} G_l(\mathbf{x}_i-\mathbf{x}_0)q(\mathbf{x}_i)ds(\mathbf{x}_i) \tag{20}$$

where N represents the number of discretization points and $ds(\mathbf{x}_i) = \frac{1}{2}(|\mathbf{x}_{i+1} - \mathbf{x}_i| + |\mathbf{x}_{i-1} - \mathbf{x}_i|)$ is the surface element associated with the point $\mathbf{x}_i$.

5.2. **Notation**

Since for every harmonic function u there exists an analytic function w for which $u = \Re(w)$, we will use complex analysis to simplify the notation. In this case, $\nabla u = (u_x, u_y) = (\Re(w'), -\Im(w'))$

5.3. **Multipole expansion**

Using the notation above, a straightforward calculation shows that the effect of any set of N points $(z_i)_{1 \leq i \leq N}$ on the surface (or contour) γ of strengths $q_i, i = 1...N$ located inside a circle C_1 of center z_c and radius r, on any point z_0 outside the circle C_1 is given by:

$$\Psi(z_0) = Q \ln(z_0 - z_c) + \sum_{k=1}^{\infty} \frac{a_k}{(z_0 - z_c)^k} \tag{21}$$

where

$$Q = \sum_{i=1}^{N} q_i \qquad \text{and} \qquad a_k = \sum_{i=1}^{N} \frac{-q_i (z_i - z_c)^k}{k}$$

Note that the terms of the series above (equation (21)) separate into a product of a coefficient depending on the source point alone (a_k depends on $q_i(z_i - z_c)$) and a function depending on the evaluation point alone, namely $(z_0 - z_c)^{-k}$. At this stage, the number of operations performed is about $O(N \log N)$.
Indeed we truncate the series in equation (21) at an order $p << N$ (p is the truncation order). For each point $\mathbf{x}_0$ we go through the tree (figure 7) and evaluate the truncated series above. Since the depth of the tree is $L \sim O(\log N)$ (due to domain subdivisions, at each level we subdivide by 4, so that at the finest level L, the number of box is 4^L, each box contains an average of s discretization points)

The main goal of the next section is to reach the $O(N)$ operations. For that purpose, multipolar moments a_k obtained from the previous step are converted into local moments. Indeed, some forms of translation and conversion will be used to make these changes. A complete proof can be found in [26, 28].

5.4. **Local expansion**

We keep the same hypothesis of the previous section, and we suppose that $|z_c| > (c+1)r$ with $c > 1$. Then the multipole expansion (21) converges inside a circle C_2 of radius r centered at the origin, and we have:

$$\Psi(z_0) \quad = \quad \sum_{l=0}^{\infty} b_l z_0^l$$

where

$$b_0 = a_0 \ln(-z_c) + \sum_{k=1}^{\infty} \frac{a_k}{z_c^k}(-1)^k \qquad \text{and} \qquad b_l = -\frac{a_0}{l \cdot z_c^l} + \frac{1}{z_c^l} \sum_{k=1}^{\infty} \frac{a_k}{z_c^k} \binom{l+k-1}{k-1} (-1)^k$$

The series is truncated to the same order p used for the multipole expansion. In comparison with the previous section we have factorized the series as a product of two coefficients, one depending on a given point z_0 where the effect is to be calculated, and the other depending on z_c where the moment is to be evaluated. In some

sense the operation consists now of regrouping elementary charges (in the electrostatics language) to build a multipole moment in a certain area. A set of charges at distant point is also regarded now as a multipole moment. The resulting interaction is thus between multipoles. In this procedure we go directly to the finest level of the tree (and not by recursive calculus) and compute the desired information in the local moment b_l for the far field calculation. We thus circumvent the tree subdivision which goes like $O(log(N))$, so that we achieve an algorithm $O(N)$.

5.5. **Numerical Results**

We present here some numerical results obtained by the FMM method and comparison is made with the direct method. In comparison with the direct implementation of BIM, that attains a limit of storage at $O(10^4)$, the present method based on FMM-BIM attains storage limit of about $O(10^7)$. The cpu time of the FMM method in comparison with the classic calculus of the BIM is illustrated in figure 8. We can observe how FMM method becomes convenient at a discretization point number $N \approx 10^3$, which is a value that will normally be used in simulations of a suspension with only few vesicles. The implementation of the method achieves high accuracy (see figure 11) at a reasonable cost. The comparison of the dynamical results are shown in figures 9 and 10: the approximation error made by the fast multipole method is lower than the estimated overall accuracy of the dynamical evolution.

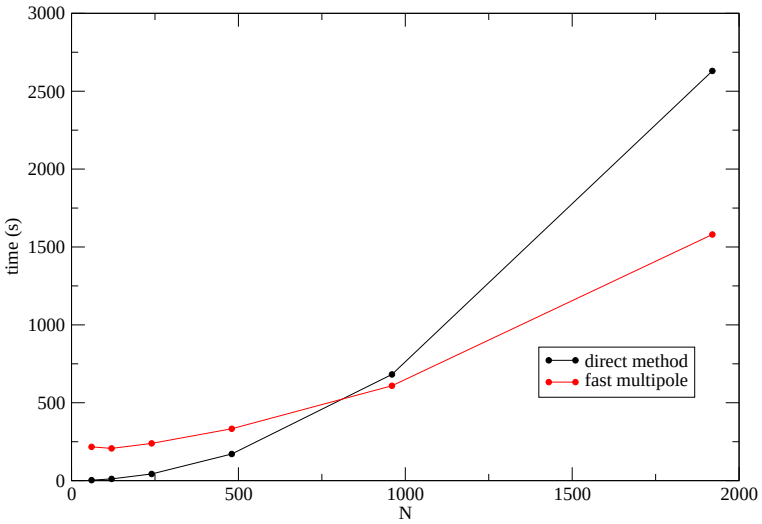

FIGURE 8. CPU time of the direct calculus and the scheme $O(N)$ versus the discretisation points N for the level 3 of the tree (time related to $2 \cdot 10^5$ time steps).

The above method has been implemented for vesicles and tests are now being performed. We hope to report along these lines in the near future by investigating a large number of vesicles.

6. CONCLUSION

The high deformation limit of a vesicle has been studied numerically for the first time. We presented results on the dynamics and rheology of a dilute suspension of two-dimensional vesicles, and have provided interpretations able to link the microscopic dynamics to the rheological behaviour. We have found a flow alignment even in the absence of viscosity contrast.

In the limit of high deformation no analytical work is available, due to the large deviation from a spherical shape (circle in two dimensions). It is worth noting that at small enough α the vesicle is close to self intersection,

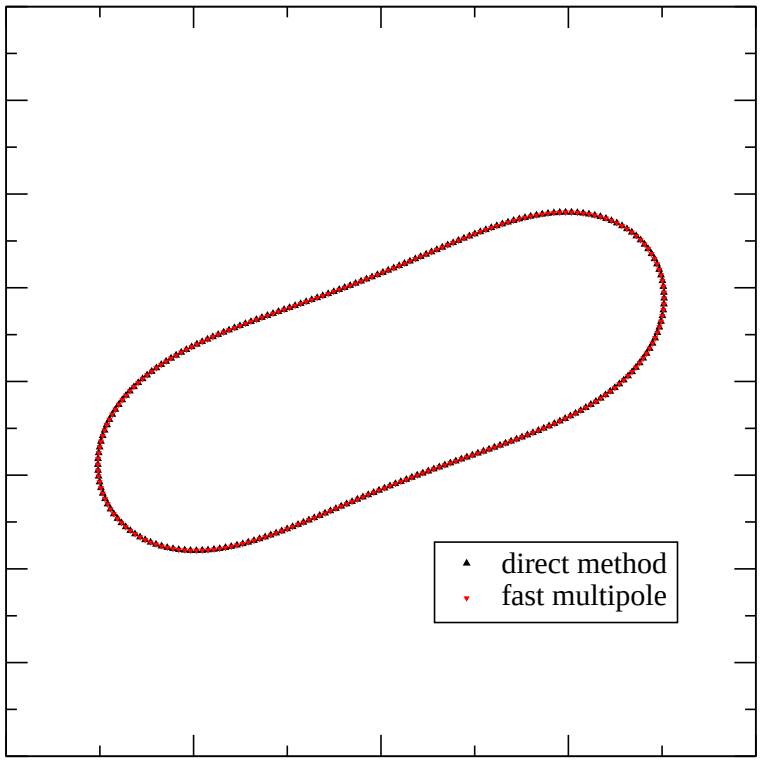

FIGURE 9. The stationary shape of a vesicle (after $2 \cdot 10^5$ time steps) by the two methods: direct computation and fast multipole ($N = 240$).

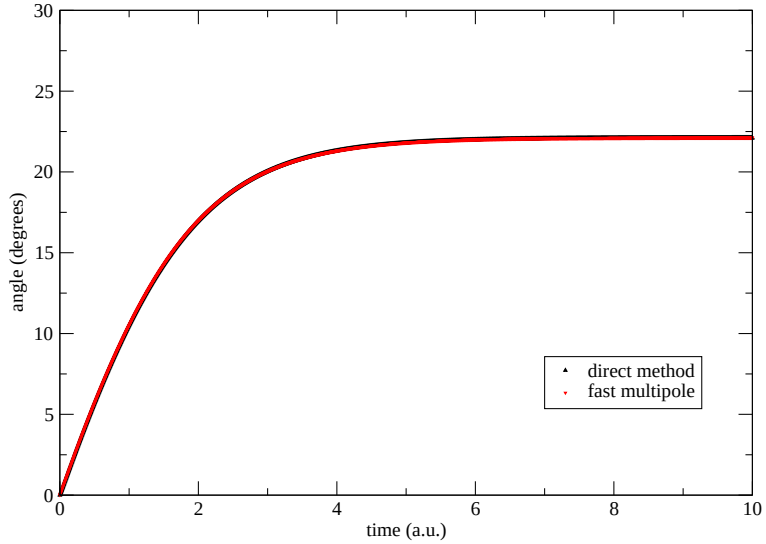

FIGURE 10. Inclination angle (in degrees) of a tank-treading vesicle in a shear flow given by the two methods for $2 \cdot 10^5$ time steps.

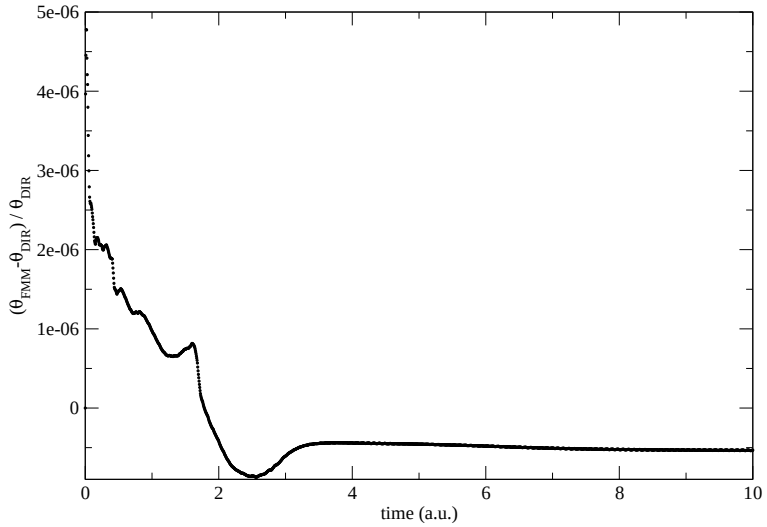

FIGURE 11. The difference of the inclination angle Θ (in degrees) of a tank-treading vesicle in a shear flow for $2 \cdot 10^5$ time steps.

so that a classical asymptotic analysis, based on the description of the position of the membrane via angular functions, might even not be possible due to the lack of uni-value representation.

Experimentally, only quite swollen vesicles have been studied so far. Having deflated vesicles may be achieved thanks to temperature increase or by osmosis. However, quite deflated vesicles are known to be often mechanically fragile in that they can easily undergo rupture. It is an interesting experimental task for future investigations to seek phospholipidic systems with the aim of circumventing this problem.

On the numerical optimization side, fast multipole method is an extremely promising technique: it will be exploited in the near future to study the dynamics and rheology of concentered suspensions. In fact the boundary integral method, despite the advantage of computing sub-dimensional integrals for the time evolution, in its direct implementation it leads to a $\mathbf{O}(N^2)$ algorithm. This entails huge computational times when the size of the system increases (semi-dilute and concentrated suspensions). FMM circumvents this limitation, allowing thus simulation of suspensions with hundreds of vesicles (or with fewer vesicles with very refined meshes), without compromising the precision of the results.

A. Analytical solution around a circle

The velocity field $\mathbf{u}$ around a circular (2D) particle embedded in a linear shear flow can be computed analytically in the Stokes regime [22, 23]. This is quite useful in order to compare the behaviour of the vesicle to the reference case of a rigid circle. Moreover it is used to test the precision of the code in the circular limit, since in this limit the vesicle behaves as a rigid (circular) body.

The radius of the particle is supposed to be equal to unity and the shear rate is denoted $\dot{\gamma}$.
We use polar coordinates (r, θ) centered on the particle, with the imposed velocity along the direction $\theta = 0, \pi$. For the boundary conditions, we impose pure linear shear flow at infinity and no-slip conditions on the surface of the particle, which is freely rotating.

The boundary conditions, expressed in polar coordinates, are:

$$\begin{aligned} u_r(r=\infty,\theta) &= \frac{\dot\gamma}{2} r \sin 2\theta \\ u_\theta(r=\infty,\theta) &= -\frac{\dot\gamma}{2} r(1-\cos 2\theta) \\ u_r(r=1,\theta) &= 0 \\ \frac{\partial u_\theta}{\partial \theta}(r=1,\theta) &= 0 \end{aligned} \tag{22}$$

It is a simple matter to show that the following set of solutions u_r, u_θ, p solves the Stokes problem with the above boundary conditions:

$$\begin{aligned} u_r(r,\theta) &= \dot\gamma \left[\frac{r}{2} - \frac{1}{r} + \frac{1}{2r^3}\right] \sin 2\theta \\ u_\theta(r,\theta) &= \dot\gamma \left[\left(\frac{r}{2} - \frac{1}{2r^3}\right)\cos 2\theta - \frac{r}{2}\right] \\ p(r,\theta) &= -\dot\gamma \frac{2}{r^2} \sin 2\theta \end{aligned} \tag{23}$$

Due to linearity of the Stokes equations, and to the fact that the shape is fixed, the solution is unique. Note that at $r=1$, we have $u_\theta = -\dot\gamma/2$.

The authors acknowledge fruitful discussions with S. K. Veerapaneni, and thank the organizers of CEMRACS, and CIRM for the hospitality. C.M. acknowledges financial support from CNES (Centre National d'Etudes Spatiales) and from ANR MOSICOB.

References

[1] S. Chien. Red cell deformability and its relevance to blood flow. *Annu. Rev. Physiol.*, 49:177–192, 1987.
[2] A. S. Popel and P. C. Johnson. Microcirculation and hemorheology. *Ann. Rev. Fluid Mech.*, 37:43–69, 2005.
[3] S. Keller and R. Skalak. Motion of a tank-treading ellipsoidal particle in a shear flow. *J. Fluid Mech.*, 120:27–47, 1982.
[4] M. Kraus, W. Wintz, U. Seifert, and R. Lipowsky. Fluid vesicles in shear flow. *Phys. Rev. Lett.*, 77:3685–3688, 1996.
[5] A. Einstein. Eine neue bestimmung der moleküldimensionen. *Ann. Phys.*, 19:289–306, 1906.
[6] A. Einstein. Berichtigung zu meiner arbeit: Eine neue bestimmung der moleküldimensionen. *Ann. Phys.*, 34:591–592, 1911.
[7] C. Misbah. Vacillating breathing and tumbling of vesicles under shear flow. *Phys. Rev. Lett.*, 96:028104, 2006.
[8] G. Danker and C. Misbah. Rheology of a dilute suspension of vesicles. *Phys. Rev. Lett.*, 98:088104, 2007.
[9] T. Biben and C. Misbah. Tumbling of vesicles under shear flow within an advected-field approach. *Phys. Rev. E*, 67:031908, 2003.
[10] I. Cantat, K. Kassner, and C. Misbah. Vesicles in haptotaxis with hydrodynamical dissipation. *Eur. Phys. J. E*, 10:175189, 2003.
[11] J. Beaucourt, T. Biben, and C. Misbah. Optimal lift force on vesicles near a compressible substrate. *Europhys. Lett.*, 67:676–682, 2004.
[12] S. K. Veerapaneni, D. Gueyffier, D. Zorin, and G. Biros. A boundary integral method for simulating the dynamics of inextensible vesicles suspended in a viscous fluid in 2d. *J. Comp. Phys.*, 228:23342353, 2009.
[13] H. Noguchi and G. Gompper. Fluid vesicles with viscous membranes in shear flow. *Phys. Rev. Lett.kantsler*, 93:258102, 2004.
[14] T. Biben and C. Misbah. An advected-field method for deformable entities under flow. *Eur. Phys. J. B*, 29:311–316, 2002.
[15] E. Maitre, T. Milcent, G.-H. Cottet, A. Raoult, and Y. Usson. Applications of level set methods in computational biophysics. *Math. Comput. Model.*, 49:21612169, 2009.
[16] I. Cantat and C. Misbah. Dynamics and similarity laws for adhering vesicles in haptotaxis. *Phys. Rev. Lett.*, 83(1):235–238, Jul 1999.
[17] V. Kantsler and V. Steinberg. Orientation and dynamics of a vesicle in tank-treading motion in shear flow. *Phys. Rev. Lett.*, 95:258101, 2005.

[18] M.-A. Mader, V. Vitkova, M. Abkarian, A. Viallat, and T. Podgorski. Dynamics of viscous vesicles in shear flow. *Eur. Phys. J. E*, 2006.
[19] B. Kaoui, G. Ristow, I. Cantat, C. Misbah, and W. Zimmermann. Lateral migration of a 2d vesicle in unbounded poiseuille flow. *Phys. Rev. E*, 77:021903, 2008.
[20] C. Pozrikidis. *Boundary Integral and Singularity Methods for Linearized Viscous Flow*. Cambridge University Press, Cambridge, UK, 1992.
[21] C. Pozrikidis. Interfacial dynamics for stokes flow. *J. Comput. Phys*, 169:250–301, 2001.
[22] R. G. Cox, I. Y. Z. Zia, and S. G. Mason. Particle motions in sheared suspensions. xxv. streamlines around cylinders and spheres. *J. Colloid. Interface Sci.*, 27(1):12, 1968.
[23] M. Belzons, R. Blanc, J.-L. Bouillot, and C. Camion. Viscosité d'une suspension diluée et bidimensionnelle de sphères. *C. R. Acad. Sc. Paris, série II*, 292:5, 1981.
[24] J. Brady. The einstein viscosity correction in n dimensions. *Int. J. Multiphase Flow*, 10:113–114, 1984.
[25] G. Danker, T. Biben, T. Podgorski, C. Verdier, and C. Misbah. Dynamics and rheology of a dilute suspension of vesicles: Higher-order theory. *Phys. Rev. E*, 76:041905, 2007.
[26] L. Greengard and V. Rokhlin. A fast algorithm for particle simulations. *J. Comp. Phys.*, 73:325–348, 1987.
[27] N. A. Gumerov and R. Duraiswami. Fast multipole method for the biharmonic equation in three dimensions. *J. Comp. Phys.*, 215(1):363 – 383, 2006.
[28] L. Greengard and V. Rokhlin. On the effficient implementation of the fast multipole algorithm. Technical report, Yale University, Department of Computer Science, 1988.